

Multiphonon resonant Raman scattering predicted in LaMnO_3 from the Franck-Condon process via self-trapped excitons

Vasili Perebeinos* and Philip B. Allen

Department of Physics and Astronomy, State University of New York, Stony Brook, New York 11794-3800

(Received 31 January 2001; published 8 August 2001)

Resonant behavior of the Raman process is predicted when the laser frequency is close to the orbital excitation energy of LaMnO_3 at 2 eV. The incident photon creates a vibrationally excited self-trapped “orbition” state from the orbitally ordered Jahn-Teller (JT) ground state. Trapping occurs by local oxygen rearrangement. Then the Franck-Condon mechanism activates multiphonon Raman scattering. The amplitude of the n -phonon process is first order in the electron-phonon coupling g . The resonance occurs *via* a dipole forbidden d to d transition. We previously suggested that this transition (also seen in optical reflectivity) becomes allowed because of asymmetric oxygen fluctuations. Here we calculate the magnitude of the corresponding matrix element using local spin-density functional theory. This calculation agrees to better than a factor of two with our previous value extracted from experiment. This allows us to calculate the absolute value of the Raman tensor for multiphonon scattering. Observation of this effect would be a direct confirmation of the importance of the JT electron-phonon term and the presence of self-trapped orbital excitons, or “orbitons.”

DOI: 10.1103/PhysRevB.64.085118

PACS number(s): 78.30.Hv, 75.30.Vn, 71.35.Aa

I. INTRODUCTION

Manganese oxide materials attract attention because of the “colossal magnetoresistance” (CMR) phenomenon,¹ and because of a very rich phase diagram² of ground states with competing order parameters. The Mn^{+3} ion of the parent LaMnO_3 compound has d^4 (t_{2g}^3, e_g^1) configuration with an inert t_{2g} core (spin 3/2). The half-filled doubly degenerate e_g orbitals ($d_{x^2-y^2}$, $d_{3z^2-r^2}$) are Jahn-Teller (JT) unstable. A symmetry-breaking oxygen distortion (resulting in the Mn-O bond lengths of 1.91, 2.18 and 1.97 Å (Ref. 3)] lowers the energy of the occupied orbital. The corresponding orbitally ordered state sets in at $T_{\text{JT}}=750$ K with x - and y -oriented e_g orbitals in the x - y plane with wave vector $\vec{Q}=(\pi, \pi, 0)$.⁴ The orbital order drives antiferromagnetic (A -type) spin order⁵ below the Neel temperature $T_N=140$ K.

There is still controversy about the origin of the orbitally ordered state. Strong electron-electron correlations may lead to orbital order *via* the superexchange interaction⁶ which lifts degeneracy of the e_g states.⁷ In another scenario proposed by Millis⁸ the Jahn-Teller electron-phonon (e -ph) interaction g ⁹ causes the orbital order and contributes to CMR. Extensive numerical work by Dagotto *et al.*¹⁰ showed that the two approaches give qualitatively similar answers. We prefer a model where the JT interaction g plus large Hubbard U and Hund energy J_H leads to single occupancy of the Mn e_g levels and a gap to on-site d to d excitations, rather than assigning the gap purely to Coulomb interactions as in a multiorbital Hubbard model. We believe that the importance of the JT interaction is evident at low hole doping of $\text{La}_{1-x}\text{Sr}_x\text{MnO}_3$, whose insulating nature is naturally explained by formation of the anti-Jahn-Teller polarons.¹¹

In this paper we present a detailed prediction of resonant multiphonon Raman features, whose observation would be a direct measure of the importance of the JT electron-phonon term. When the oscillator potential curves of ground and excited states are displaced relative to each other, then vibra-

tional Raman scattering is activated by a Franck-Condon (FC) two-step mechanism. Our Hamiltonian for LaMnO_3 , with $U \rightarrow \infty$, leads to a picture where the ground state and low-lying excited states are simple products of localized orbitals, one per atom. In the first step of the FC Raman process, the incident photon creates an orbital defect in the ordered JT ground state (one Mn ion has the upper rather than the lower state of the JT doublet occupied.) This Frenkel exciton (also called an “orbition”) is self-trapped¹² by oxygen rearrangement from the JT state. The FC principle has the oxygen positions undistorted during optical excitation, producing a vibrationally excited state of the orbition. In the second step of the Raman process, this virtual excitation decays back to the orbital ground state, but not necessarily the vibrational ground state. The amplitude for ending in a vibrationally excited state is determined by displaced-oscillator overlap integrals. This allows n -phonon resonant Raman scattering with amplitude proportional to the first order of the e -ph interaction.^{13,14} The process is illustrated in Fig. 1. In the conventional Raman scattering process, where electronically excited states do not alter atomic positions, the amplitude of the n -phonon peak is proportional to the n th order of the e -ph interaction which is smaller by $n-1$ orders of magnitude. The conventional process can be divided into three steps. (1) The incident photon creates an electron-hole pair (or exciton). (2) This electron-hole pair is scattered into another state by sequential emission of n phonons via n powers of the e -ph interaction $\mathcal{H}_{e\text{-ph}} \propto g$. Higher-order interactions, such as the electron-(two phonon) interaction also enter, but do not increase the order of magnitude of the process. (3) The electron-hole pair recombines, emitting a scattered photon. In this formulation, the intensity of the two-phonon Raman process is smaller than one-phonon by several orders of magnitude 10^{-2} – 10^{-3} , determined by the $2n$ -th power of the ratio of e -ph to electronic energies.

II. FRANCK-CONDON MECHANISM

We use a model Hamiltonian,¹¹ the same as used by Millis¹⁵ (except that we have $U = \infty$), with two e_g orbitals

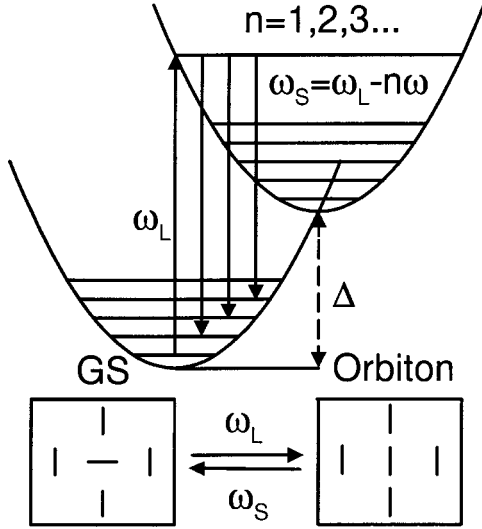


FIG. 1. Schematic Franck-Condon mechanism for the multiphonon Raman process via the orbiton intermediate state. The lowest energy configuration of the orbiton has energy Δ and large oxygen distortions from the JT ground state (GS). The most probable intermediate state (the strongest resonance of the Raman process) occurs at $\omega_L \approx 2\Delta \approx 2$ eV, rather than $\omega_L = \Delta$.

per Mn atom, fully respecting the symmetries of the orbitals and the crystal. The electron-phonon term \mathcal{H}_{JT} stabilizes the orbitally ordered ground state via a cooperative JT distortion. Oxygen displacements along Mn-O-Mn bonds are modeled by local Einstein oscillators

$$\begin{aligned} \mathcal{H}_{JT} &= -g \sum_{l,\alpha} \hat{n}_{l,\alpha} (u_{l,\alpha} - u_{l,-\alpha}), \\ \mathcal{H}_L &= \sum_{l,\alpha} (P_{l,\alpha}^2/2M + Ku_{l,\alpha}^2/2). \end{aligned} \quad (1)$$

The interaction \mathcal{H}_{JT} consists of linear energy reduction of an occupied $d_{3x^2-r^2}$ orbital [the corresponding creation operator

is c_x^\dagger and number operator is $\hat{n}_{l,x} = c_x^\dagger(l)c_x(l)$] if the two oxygens in the $\pm \hat{x}$ direction expand outwards. Similar terms are included for \hat{y} and \hat{z} oxygens if $d_{3y^2-r^2}$ or $d_{3z^2-r^2}$ orbitals are occupied. The strength $g = 1.84$ eV/Å of the JT coupling g determines the JT splitting of the orbitals $2\Delta = 1.9$ eV, and was chosen to agree with the lowest optical conductivity peak.^{16,17} The displacement $u_{l,\alpha}$ is measured from the cubic perovskite position of the nearest oxygen in the $\hat{\alpha}$ direction to the Mn atom at l . The oxygen vibrational energy $\hbar\omega = \hbar\sqrt{K/M} = 0.075$ eV is taken from a Raman experiment.¹⁸ In addition there is an on site Coulomb repulsion U and a large Hund energy J_H . In the limit $U \rightarrow \infty$ and $J_H \rightarrow \infty$, electronic motion at half-filling is suppressed due to single occupancy of the Mn sites; additional orbital splitting caused by superexchange interactions is left out.

The Hamiltonian $\mathcal{H} = \mathcal{H}_{JT} + \mathcal{H}_L$ gives an orbitally ordered ground state

$$|0,0\rangle = \prod_l^A c_X^\dagger(l) \prod_{l'}^B c_Y^\dagger(l') |\{0\}\rangle, \quad (2)$$

where $\{0\}$ refers to the lattice vibrational ground state with oxygen atoms in distorted equilibrium positions (Van Vleck Q_2 -type distortions) $u_{l\pm x} = \pm u_0, u_{l\pm y} = \mp u_0, u_{l\pm z} = 0$ if $l \in A$ sublattice [$\exp(i\vec{Q}\cdot\vec{l}) = 1$] and opposite sign distortions if $l \in B$ sublattice [$\exp(i\vec{Q}\cdot\vec{l}) = -1$]. The magnitude of the distortion $2u_0 = \sqrt{2\Delta/M\omega^2} = 0.296$ Å agrees with neutron diffraction data³ within 10–15 %, confirming that the model has sufficient resemblance to reality. Operators $c_{X,Y}^\dagger$ create electrons with orbitals $\Psi_{X,Y} = -(d_{3z^2-r^2} \mp d_{x^2-y^2})/\sqrt{2}$ alternating on A and B sublattices. The lowest-lying electronic excitation of the Hamiltonian (1) is a self-trapped exciton or orbiton,¹² which gives a broad line in the optical conductivity^{16,17} centered at $2\Delta \approx 2$ eV.

In the n -phonon Raman process, incident light of frequency ω_L is scattered with a shifted frequency $\omega_S = \omega_L - n\omega$. The Raman cross-section tensor \mathbf{R}^n can be found as follows:¹⁹

$$\frac{\partial^2 \mathbf{R}^n}{\partial \omega_R \partial \Omega} = \frac{\sigma_0}{m_e^2} \frac{\omega_S^2}{\omega_L^2} \left| \sum_{\{m\},i} \frac{\langle 0,n | \hat{\epsilon}_L \cdot \hat{p} | i, m \rangle \langle i, m | \hat{\epsilon}_S \cdot \hat{p} | 0,0 \rangle}{\Delta + N\{m\}\hbar\omega - \hbar\omega_L + i\gamma_m} + \text{NRT} \right|^2 \delta(\omega_R - n\omega), \quad (3)$$

where $\sigma_0 = r_e^2$ is the Compton cross section ($r_e = e^2/m_e c^2$). The summation goes over all electronic states i and all the corresponding vibrational quanta $\{m\}$. $N\{m\} = m_x + m_y + m_z + m_{-x} + m_{-y} + m_{-z}$ is the total number of vibrational quanta. The nonresonant term (NRT) is obtained from the resonant term by permuting $\hat{\epsilon}_L$ with $\hat{\epsilon}_S$ and changing $-\omega_L$ to ω_S . The imaginary frequency γ_m gives a broadening which can mimic the effect of phonon dispersion. The final state $|0,n\rangle$ has an electronic ground state plus n vibrational quanta. Summation over all the possible states with a total number of n vibrations is assumed in Eq. (3). For example,

one phonon can be excited on any of the six neighboring oxygen atoms; two phonons can be excited in 21 ways; three phonons in 56 ways, and so on. The ground state couples to excited electronic states by the electron-radiation Hamiltonian ($\hat{p} \cdot \vec{A}$). In LaMnO₃, we consider only the lowest excited electronic state with an orbital flip (e.g., $|X\rangle$ type to $|Y\rangle$ type¹¹). By neglecting coupling to higher electronic states we underestimate (perhaps by a significant factor) the first order Raman peak intensity. For multiphonon Raman scattering, in first approximation, we assume that only orbiton intermediate states contribute.

III. LSDA DIPOLE MATRIX ELEMENTS

To evaluate dipole matrix elements in Eq. (3) we use the FC approximation. The wave functions $|0,0\rangle$, $|i,m\rangle$, and $|0,n\rangle$ are written as products of vibrational wave functions $\chi(\vec{R})$ dependent on the oxygen positions \vec{R} , and electronic wave functions $\psi(\vec{r},\vec{R})$ dependent on both electronic \vec{r} and vibrational coordinates. The electronic dipole matrix element is a d to d transition and therefore forbidden when the surroundings are symmetric. Searching for a mechanism to activate this transition, we notice that an asymmetric oxygen displacement will cause Mn e_g orbitals to acquire an admixture of $4p$ character. A typical mixing coefficient is

$$\gamma_z = \int d\vec{r} \psi_{3z^2-r^2} \frac{\partial V}{\partial u_z} \psi_z / (\epsilon_d - \epsilon_p), \quad (4)$$

where ψ_z is an orbital of p character, and $\partial V/\partial u_z$ is the perturbation caused by a displacement of oxygen $l + \hat{z}$ in \hat{z} direction. The corresponding allowed optical matrix element is

$$p_z = \int d\vec{r} \psi_{3z^2-r^2} \hat{p}_z \psi_z. \quad (5)$$

The resulting dipole matrix element is

$$\langle i, m | \hat{\epsilon}_{S,L} \cdot \hat{p} | 0, n \rangle = \sum_{\alpha=x,y,z} \gamma_\alpha p_\alpha \epsilon_\alpha \langle m_x m_x m_y m_y m_z m_z | (u_\alpha + u_{-\alpha}) | n_x n_x n_y n_y n_z n_z \rangle. \quad (6)$$

If the ground state is described by Eq. (2), then from symmetry one can show that $\gamma_x p_x = \gamma_y p_y = -\gamma_z p_z/2$. In our previous work¹² a phenomenological parameter $\gamma d \approx -\gamma_z p_z (\hbar/2m_e \Delta)$ was introduced to account for the observed spectral weight of the optical conductivity peak due to the self-trapped exciton. The oscillator strength f defined as $\int d\omega \sigma(\omega) = (\pi N e^2 / 2m_e \Omega) f$ is equal in our model to $f_{zz} = 2[(\gamma_z p_z)^2 / m_e M \omega^2] / (2\Delta/\hbar \omega + 1)$, and $f_{xx} = f_{yy} = f_{zz}/4$. Here N/Ω is the Mn atom concentration. The measured spectral weight $540\Omega^{-1} \text{cm}^{-1} \text{eV}$ of the lowest broad line centered at 2 eV (Ref. 16) corresponds to $f_{\text{exp}} = 0.113$ or $\gamma_z p_z = 1.7(m_e M \omega^2)^{1/2}$ (the spectral weight $740\Omega^{-1} \text{cm}^{-1} \text{eV}$ under a Lorentzian fit¹⁷ corresponds to $f_{\text{exp}} = 0.16$). Here we use density functional theory (DFT) to calculate an induced dipole matrix elements to test whether our choice of the parameter $\gamma_z p_z$ from the optical data was justified.

LaMnO₃ has been extensively studied by first-principles approaches²⁰ including the local-spin-density approximation (LSDA) of DFT, LDA+U, and Hartree-Fock methods. Information about electronic and magnetic structure, and about electron-phonon and Coulomb interactions has been obtained. Here we use LSDA to calculate the dipole matrix element for d to d transitions as it is induced by asymmetric oxygen distortions. Rather than calculating $\partial V/\partial u_z$ and doing perturbation theory as in Eqs. (4),(5), we directly calculate $\langle i | \epsilon \cdot \hat{p} | 0 \rangle$ in the presence of an imposed asymmetric oxygen distortion.

To solve the LSDA equations we use the plane-wave pseudopotential method^{21,22} with a spin-dependent exchange-correlation potential²³ and a supercell approach. Calculations were done for a 10-atom perovskite supercell with only Q_2 -type JT oxygen distortions (the rotation of the MnO₆ octahedra is omitted.) The point group symmetry of the cell is thus D_{4h} . For convenience, the magnetic order is taken to be ferromagnetic with $4.00\mu_B$ spin magnetization per for-

mula unit. The lattice constant 3.936 \AA gives the same cell volume as observed for LaMnO₃. The magnitude of the in-plane oxygen distortions along the Mn-O-Mn bonds is $u_0 = 0.14 \text{ \AA}$. The self-consistent charge density was calculated using six special \mathbf{k} points in the irreducible wedge of the Brillouin zone. First, the k points were chosen on the undistorted cubic structure Brillouin zone. Then they were mapped into the tetragonal Q_2 -type JT distorted Brillouin zone. The resulting k -point sampling would give the cubic symmetry charge density for the undistorted cubic LaMnO₃ calculated in the tetragonal (doubled) unit cell. The symmetry broken charge density is obtained because of the oxygen distortions not because of the k -points sampling.²⁴ Then the self-consistent potential was used to calculate wavefunctions at the Γ point.

A symmetry analysis of the pseudo wave functions for $\mathbf{k} = (0,0,0)$ and plots of $|\psi|^2$ around the Mn site allow us to distinguish Mn e_g states from other states. The e_g (X - and Y -type) orbitals form states of A_{1g} and B_{1g} symmetries. Two of the four Mn e_g states are shown on Fig. 2. By introducing a small displacement of all the apical oxygens in $+\hat{z}$ direction along the Mn-O-Mn bonds, one induces a p_z dipole matrix element (A_{1g} to A_{1g} and B_{1g} to B_{1g}). Similarly, in-plane oxygen displacement in the $+\hat{x}$ direction induces a p_x matrix element. In Table I we present LSDA results for these matrices. The imposed displacement has lowered the D_{4h} symmetry of the supercell, permitting transitions between states below and above the Fermi level which were previously labeled as A_{1g} and B_{1g} . The energies of the Mn e_g states do not alter much (less than 0.04 eV) for small distortions (0.016 \AA) and the induced dipole matrix elements are linear with oxygen distortion.

It is convenient to measure the induced dipoles in units of $(m_e M \omega^2)^{1/2} = 0.472\hbar/(a_B)^2$, where m_e and M are electron and oxygen masses and a_B is the Bohr radius. The calculated dipoles $(\gamma p)_z = 2.33$ and $(\gamma p)_{x,y} = 1.55$ give the oscillator

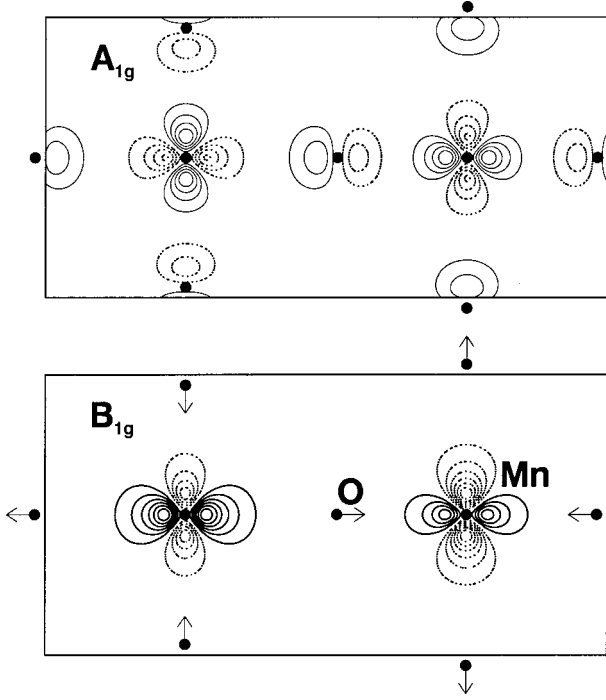


FIG. 2. The LSDA wave functions $\Psi(\vec{r})$ at $\vec{k}=(0,0,0)$ point for the Mn e_g states B_{1g} (occupied) and A_{1g} (empty). Arrows indicate the direction of the Q_2 -type oxygen displacements in the xy plane. Negative (dashed) and positive (solid) contour values are in units of $0.1 e^{1/2}/(\text{a. u.})^{3/2}$

strengths $f_{zz}=0.41$ and $f_{xx,(yy)}=0.18$. These answers are somewhat larger than experiment, but well within the expected accuracy of our model. This accuracy is limited by four factors: (1) convergence of the LSDA result; (2) neglect of rotational distortions; (3) simplification of magnetic structure to ferromagnetic; and (4) applicability of LSDA to strongly correlated electrons. We tested the first by varying the number of plane waves used in the pseudopotential expansion. The answers reported here used a plane-wave cutoff $E_{pw}=135$ Ry. The value of $\gamma_z p_z$ increases by 9% at $E_{pw}=120$ Ry and decreases by 13% at $E_{pw}=100$ Ry, so the convergence error is estimated at 10%. To calculate dipole matrix elements we used pseudowave functions, which are different from the physical wave functions in the core

TABLE I. The absolute values of the induced dipole matrix elements p_z (left) and p_x (right) per unit oxygen displacements in units of $(m_e M \omega^2)^{1/2}$ between the LSDA wave functions of the A_{1g} and B_{1g} symmetry before an additional asymmetric oxygen distortion. The resulting oscillator strengths for the transition between the occupied (occ) and empty (em) states are $f_{zz}=0.41$ and $f_{xx,(yy)}=0.18$, which corresponds to $(\gamma p)_z=2.33$ and $(\gamma p)_{x,y}=1.55$.

	A_{1g}^{occ}	A_{1g}^{em}	B_{1g}^{occ}	B_{1g}^{em}	A_{1g}^{occ}	A_{1g}^{em}	B_{1g}^{occ}	B_{1g}^{em}
A_{1g}^{occ}	0	3.29	0	0	0	1.33	1.32	0.69
A_{1g}^{em}	3.29	0	0	0	1.33	0	1.39	0.06
B_{1g}^{occ}	0	0	0	0.16	1.32	1.39	0	0.78
B_{1g}^{em}	0	0	0.16	0	0.69	0.06	0.78	0

region.²⁵ The introduced error depends on the cutoff radius used for the construction of pseudopotential²² and gives 5% discrepancy for the radial part of the \hat{p} -operator using pseudo and real wave functions of an isolated Mn atom. Sources (2) and (3) will cause errors of similar size as source (1), we believe. The biggest uncertainty is source (4). In transition metals, the energy levels of the localized d states are significantly altered if one includes explicit additional Coulomb repulsion of localized states as in the LDA+U approach.²⁶ Wave functions and matrix elements could also change perhaps by as much as a factor of 2. However, this would not change our qualitative conclusion. This calculation gives us extra confidence that phonon-activation is strong enough to account for the observation of d to d (orbital) transitions in optical reflectivity, as we assumed in our previous work, and as we now use to predict Raman spectra.

IV. THE RAMAN TENSOR

The absolute cross sections for the Raman process Eq. (3) can be evaluated using expression (6):

$$\frac{\partial^2 R_{\alpha\beta}^n}{\partial \omega_R \partial \Omega} = \sigma_0 \frac{\omega_S^2}{\omega_L^2} (\gamma_\alpha p_\alpha \gamma_\beta p_\beta)^2 \delta(\omega_R - n\omega) \sum_{\{f\}} \delta(n - N\{f\}) \times \left| \sum_{m=0}^{\infty} \frac{\hbar \omega A_{\alpha\beta}(m, \{f\})}{\Delta + m\hbar\omega - \hbar\omega_L + i\gamma_m} + \text{NRT} \right|^2, \quad (7)$$

$$A_{\alpha\beta}(m, \{f\}) = \sum_{\{m'\}} \delta(m - N\{m'\}) \langle f | u_\alpha + u_{-\alpha} | m' \rangle \times \langle m' | u_\beta + u_{-\beta} | 0 \rangle, \quad (8)$$

where the induced dipole matrix elements γp and displacements u are measured in units of $(m_e M \omega^2)^{1/2}$ and $\sqrt{\hbar/M\omega}$, respectively. In order to evaluate vibrational overlap integrals $A_{\alpha,\beta}(m, \{f\})$ one needs the expressions for overlap integrals of displaced harmonic oscillators¹³

$$\langle n_1 | n_2 \rangle = (-1)^{n_1 - n_2} \sqrt{n_1! n_2!} e^{-\kappa^2/2} \kappa^{n_1 - n_2} \times \sum_{k=0}^{n_2} (-1)^k \frac{\kappa^{2k}}{k!(n_2 - k)!(n_1 - n_2 + k)!} \quad (9)$$

if $n_1 \geq n_2$,

$$\langle n_1 | u | n_2 \rangle = \frac{\kappa}{\sqrt{2}} \left(1 + \frac{n_2 - n_1}{\kappa^2} \right) \langle n_1 | n_2 \rangle, \quad (10)$$

where κ is related to the Jahn-Teller gap as $\Delta = 4\kappa^2 \hbar \omega$. The overlap $\langle n_1 | n_2 \rangle$ for $n_1 < n_2$ has the same expression as Eq. (9) with n_1 and n_2 interchanged and the sign of the displacement $u_0 = \sqrt{2}\kappa$ changed ($\kappa \rightarrow -\kappa$). When using expressions

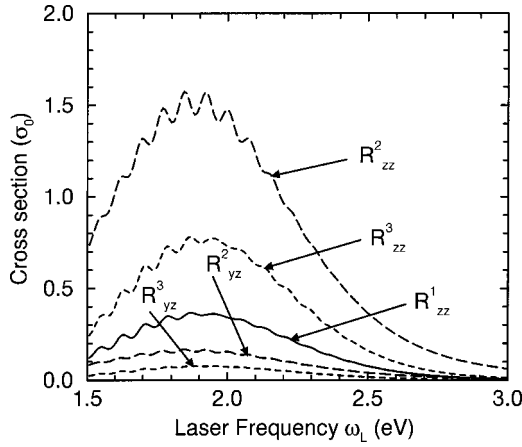


FIG. 3. The absolute value of the multiphonon Raman cross section per solid angle versus incident photon energy. Resonant behavior is predicted for ω_L close to orbiton energy $2\Delta=1.9$ eV. The damping constant is $\gamma_0=120$ cm^{-1} , the induced dipoles are $-\gamma_z d_z=2\gamma_x d_x=1.7$ ($m_e M \omega^2$) $^{1/2}$, cross section unit is $\sigma_0=(e^2/m_e c^2)^2$.

(9),(10), the signs of the $l+\hat{x}, l-\hat{y}$ oxygens displacements are positive and $l-\hat{x}, l+\hat{y}$ are negative, if $l \in A$ (reverse signs if $l \in B$) and $l \pm \hat{z}$ oxygens are undisplaced. Evaluation of the overlap integrals $A_{\alpha\beta}(m, \{f\})$ is straightforward. For example, for the first order Raman peak, only four one-phonon final states will contribute:

$$A_{\alpha\beta}(m, \{f\}=1 \dots 4) = \delta_{\alpha,\beta} \frac{e^{-\Delta} \Delta^m}{m!} \frac{m}{4\kappa\Delta} (\Delta+1-m) \quad (11)$$

with no contribution to the nondiagonal part of the tensor $\alpha \neq \beta$. For second- and third-order Raman scattering, four and eight final states contribute to the nondiagonal part of the tensor:

$$A_{xy(yz, zx)}(m, \{f\}=1 \dots 4) = \pm \frac{e^{-\Delta} \Delta^m}{m!} \frac{m}{2\Delta},$$

$$A_{xy(yz, zx)}(m, \{f\}=1 \dots 8) = \pm \frac{e^{-\Delta} \Delta^m}{m!} \frac{\kappa m}{\sqrt{2}\Delta^2} (\Delta+1-m). \quad (12)$$

The formulas for the diagonal parts of the higher-order Raman tensors are more complicated and will not be given here.

To model the damping term γ_m of vibrational level m , we use expression $\gamma_m = \gamma_0 \sqrt{m+1}$, as in a sequence of convolved Gaussians, intended to mimic the local densities of phonon states on oxygen atoms. The value $\gamma_0=120$ cm^{-1} was taken. The Raman cross section shown on Fig. 3 has a pronounced resonant behavior when the laser frequency ω_L approaches the orbiton energy 2Δ . The first-order cross section as seen in Fig. 3 is underestimated, because we neglected coupling to higher electronic levels in Eq. (7), whose contribution to multiphonon peaks is probably negligible. The polarization dependence of the cross section is only due

to the dipole matrix element effect, namely, $\mathcal{R}_{xx}^{1,2,3} = \mathcal{R}_{yy}^{1,2,3} = \mathcal{R}_{zz}^{1,2,3}/16$, $R^{2,3}_{yz} = R^{2,3}_{zx} = 4R^{2,3}_{xy}$. The anisotropy of the optical conductivity σ_{xx}/σ_{zz} is quadratic and Raman intensity $\mathcal{R}_{xx}/\mathcal{R}_{zz}$ fourth power in the dipole matrix-element anisotropy $\gamma_x p_x / \gamma_z p_z$. Actual occupied e_g orbitals may be rotations of our idealized state Eq. (2) in the e_g space. Even small deviations from Eq. (2) might cause a noticeable change of the ratio $\gamma_x p_x / \gamma_z p_z$ from the value 0.5. Therefore the predicted anisotropies of 4 and 16 for optical and Raman spectra are not necessarily robust, but the relation $\mathcal{R}_{xx}/\mathcal{R}_{zz} = (\sigma_{xx}/\sigma_{zz})^2$ should hold.

Published Raman measurements¹⁸ on undoped LaMnO_3 do not extend to the multiphonon region and resonant behavior has not been tested experimentally. Most experiments use the Ar^+ laser, for which frequency $\omega_L=2.41$ eV, we predict the multiphonon cross sections $\mathcal{R}_{zz}^2=0.514, \mathcal{R}_{zz}^3=0.243, \mathcal{R}_{yz}^2=0.056, \mathcal{R}_{yz}^3=0.025$ in units of σ_0 sr^{-1} . Recently some features in Raman spectra on LaMnO_3 around 1100 cm^{-1} were reported by several groups.²⁷⁻²⁹ These are probably the effect we are predicting.

V. CONCLUSION

We advocate a picture of the orbitally ordered state of LaMnO_3 where electron-phonon interactions (in a context of large Hund and Hubbard energies) have a major influence. Our picture is disputed by other theorists.³⁰ Therefore we attempt here to provide predictions which can qualitatively distinguish our model from others. In our model, the lowest electronic excitation is the 1.9 eV transition across the Jahn-Teller gap, modified by self-trapping to give a minimum gap half as large. This has successfully described the observed^{16,17} optical gap as a Franck-Condon broadened self-trapped exciton. The present paper uses density-functional theory to eliminate the need for a phenomenological coupling γp to account for this transition.

As a more stringent test, we here predict a new feature unique to the FC physics of the self-trapped exciton, namely, a sequence of resonant multiphonon Raman peaks. We predict the absolute values of the multiphonon Raman cross section tensors.

A hot luminescence process can also give rise to a multiphonon peaks. Incident light can excite an orbiton with a long lifetime which can recombine after vibrational energy $n\omega$ being lost in the intermediate state through anharmonic interaction. The question whether the Raman or hot luminescence mechanisms dominate the scattering intensity has an old history.³¹ In the Raman case the intensity of the higher order peaks should decrease and the width of the peak representing a convolved density of local phonon modes should increase. In the hot luminescence the intensities of the higher order peaks are of the same order and the width of the lines decrease with increasing order. In addition a strong emission peak can be observed at the exciton absorption edge. Raman techniques can serve as a direct probe of the orbiton excitation in LaMnO_3 . A recent Raman experiment³² on LaMnO_3

report a very interesting new feature above the energy of one phonon excitation. It appears not to be emission of two Jahn-Teller phonons, and has been interpreted instead as an “orbital.” This interpretation conflicts with our picture of LaMnO_3 . Further experimental study is needed. Observation of our predicted multiphonon feature would help to resolve the issue.³³

ACKNOWLEDGMENTS

We thank D. Romero for encouragement on this problem, A. J. Millis for nudging us to do DFT calculations, and M. Weinert for valuable discussions of the DFT results. This work was supported in part by NSF Grant No. DMR-0089492.

*Current address: Physics Department, Brookhaven National Laboratory, Upton, NY 11973.

¹*Colossal Magnetoresistance, Charge Ordering, and Related Properties of Manganese Oxides*, edited by C.N.R. Rao and B. Raveau (World Scientific, Singapore, 1998); *Physics of Magnetites*, edited by T. A. Kaplan and S. D. Mahanti (Kluwer Academic, New York, 1999); *Colossal Magnetoresistive Oxides*, edited by Y. Tokura (Gordon & Breach, New York, 2000).

²R. M. Kusters, J. Singelton, D. A. Keen, R. McGreevy, and W. Hayes, *Physica B* **155**, 362 (1989); S. Jin, T. H. Tiefel, M. McCormack, R. A. Fastnacht, R. Ramesh, and L. H. Chen, *Science* **264**, 413 (1994); J. M. D. Corey, M. Viret, and S. von Molnar, *Adv. Phys.* **48**, 167 (1999).

³J. Rodriguez-Carvajal, M. Hennion, F. Moussa, A. H. Moudden, L. Pinsard, and A. Revcolevschi, *Phys. Rev. B* **57**, 3189 (1998); T. Proffen, R. G. DiFrancesco, S. J. L. Billinge, E. L. Brosha, and G. H. Kwei, *ibid.* **60**, 9973 (1999).

⁴Y. Murakami, J. P. Hill, D. Gibbs, M. Blume, I. Koyama, M. Tanaka, H. Kawata, T. Arima, Y. Tokura, K. Hirota, and Y. Endoh, *Phys. Rev. Lett.* **81**, 582 (1998).

⁵F. Moussa, M. Hennion, J. Rodriguez-Carvajal, H. Moudden, L. Pinsard, and A. Revcolevschi, *Phys. Rev. B* **54**, 15 149 (1996); K. Hirota, N. Kaneko, A. Nishizawa, and Y. Endoh, *J. Phys. Soc. Jpn.* **65**, 3736 (1996).

⁶K. I. Kugel and D. I. Khomskii, *Sov. Phys. Usp.* **25**, 231 (1982).

⁷Y. Tokura and N. Nagaosa, *Science* **288**, 462 (2000).

⁸A. J. Millis, P. B. Littlewood, and B. I. Shraiman, *Phys. Rev. Lett.* **74**, 5144 (1995); A. J. Millis, B. I. Shraiman, and R. Mueller, *ibid.* **77**, 175 (1996).

⁹J. Kanamori, *J. Appl. Phys.* **31**, 14S (1960).

¹⁰T. Hotta, A. L. Malvezzi, and E. Dagotto, *Phys. Rev. B* **62**, 9432 (2000).

¹¹P. B. Allen and V. Perebeinos, *Phys. Rev. B* **60**, 10 747 (1999).

¹²P. B. Allen and V. Perebeinos, *Phys. Rev. Lett.* **83**, 4828 (1999).

¹³L. L. Krushinskii and P. P. Shorygin, *Opt. Spectrosc.* **11**, 12 (1961); **11**, 80 (1961).

¹⁴A. C. Albrecht, *J. Chem. Phys.* **34**, 1476 (1961); E. Mulazzi, *Phys. Rev. Lett.* **25**, 228 (1970); P. P. Shorygin, *Sov. Phys. Usp.* **16**, 99 (1973).

¹⁵A. J. Millis, *Phys. Rev. B* **53**, 8434 (1996).

¹⁶J. H. Jung, K. H. Kim, T. W. Noh, E. J. Choi, and J. Yu, *Phys. Rev. B* **57**, 11 043 (1998).

¹⁷J. H. Jung, K. H. Kim, D. J. Eom, T. W. Noh, E. J. Choi, J. Yu, Y. S. Kwon, and Y. Chung, *Phys. Rev. B* **55**, 15 489 (1997).

¹⁸M. N. Iliev, M. V. Abrashev, H.-G. Lee, V. N. Popov, Y. Y. Sun, C. Thomsen, R. L. Meng, and C. W. Chu, *Phys. Rev. B* **57**, 2872 (1998); V. B. Podobedov, A. Weber, D. B. Romero, J. P. Rice, and H. D. Drew, *ibid.* **58**, 43 (1998); E. Granado, J. A. Sanjurjo, C. Rettori, J. J. Neumeier, and S. B. Oseroff, *ibid.* **62**, 11 304 (2000).

¹⁹M. Cardona, in *Light Scattering in Solids II*, edited by M. Cardona and G. Güntherodt, Topics in Applied Physics No. 50 (Springer, Berlin, 1982), p. 19.

²⁰D. D. Sarma, N. Shanthi, S. R. Barman, N. Hamada, H. Sawada, and K. Terakura, *Phys. Rev. Lett.* **75**, 1126 (1995); W. E. Pickett and D. J. Singh, *Phys. Rev. B* **53**, 1146 (1996); S. Satpathy, Z. S. Popović, and F. R. Vukajlović, *Phys. Rev. Lett.* **76**, 960 (1996); I. Solovyev, N. Hamada, and K. Terakura, *ibid.* **76**, 4825 (1996); *Phys. Rev. B* **53**, 7158 (1996); D. J. Singh and W. E. Pickett, *ibid.* **57**, 88 (1998); Y.-S. Su, T. A. Kaplan, S. D. Mahanti, and J. F. Harrison, *ibid.* **61**, 1324 (2000).

²¹N. Chetty, M. Weinert, T. S. Rahman, and J. W. Davenport, *Phys. Rev. B* **52**, 6313 (1995).

²²To generate pseudopotentials [N. Troullier and J. L. Martins, *Phys. Rev. B* **43**, 1993 (1991)] we use core radii 1.6, 1.6, 3.2 a.u. for O $2s^2$, $2p^{3.5}$, $3d^{0.5}$ orbitals; 2.5, 3.0, 1.3 a.u. for Mn $4s^{1.5}$, $4p^{0.5}$, $3d^5$ orbitals; and 3.9, 4.5, 2.2 a. u. for La $6s^{1.5}$, $6p^{0.5}$, $5d^1$ orbitals with a nonlinear core correction for Mn and La. Plane wave cutoffs were $E_{pw}=135$ Ry for the wave functions and 130 Ry for the pseudopotential truncation [M. Alatalo, M. Weinert, and R. E. Watson, *ibid.* **60**, 7680 (1999)].

²³D. M. Ceperley and B. J. Alder, *Phys. Rev. Lett.* **45**, 566 (1980).

²⁴M. Weinert (private communication).

²⁵A. J. Read and R. J. Needs, *Phys. Rev. B* **44**, 13 071 (1991); H. Kageshima and K. Shiraishi, *Jpn. J. Appl. Phys.* **35**, L1605 (1996); P. Monachesi, A. Marini, G. Onida, M. Palumbo, and R. Del Sole, *Phys. Status Solidi A* **184**, 101 (2001).

²⁶A. I. Liechtenstein, V. I. Anisimov, and J. Zaanen, *Phys. Rev. B* **52**, R5467 (1995); A. B. Shick, A. I. Liechtenstein, and W. E. Pickett, *ibid.* **60**, 10 763 (1999).

²⁷P. Björnsson, M. Rübhausen, J. Bäckström, M. Käll, S. Eriksson, J. Eriksen, and L. Börjesson, *Phys. Rev. B* **61**, 1193 (2000).

²⁸D. B. Romero, Y. Moritomo, J. F. Mitchell, and H. D. Drew, *Phys. Rev. B* **63**, 132404 (2001).

²⁹A. E. Pantoja, H. J. Trodahl, A. Fainstein, R. G. Pregliasco, R. G. Buckley, G. Balakrishnan, M. R. Lees, and D. McK. Paul, *Phys. Rev. B* **63**, 132406 (2001).

³⁰J. van den Brink, P. Horsch, and A. M. Oleś, *Phys. Rev. Lett.* **85**, 5174 (2000); V. Perebeinos and P. B. Allen, *ibid.* **85**, 5178 (2000).

³¹E. F. Gross, S. A. Permogorov, V. V. Travnikov, and A. V. Sel'kin, *Fiz. Tverd. Tela* **13**, 699 (1971) [*Sov. Phys. Solid State* **13**, 578 (1971)]; M. V. Klein, *Phys. Rev. B* **8**, 919 (1973); Y. R. Shen, *ibid.* **9**, 622 (1974); T. P. Martin, *Phys. Rev.* **13**, 3618 (1976).

³²E. Saitoh, S. Okamoto, K. T. Takahashi, K. Tobe, K. Yamamoto, T. Kiumura, S. Ishihara, S. Maekawa, and Y. Tokura, *Nature (London)* **410**, 180 (2001).

³³P. B. Allen and V. Perebeinos, *Nature (London)* **410**, 155 (2001).